325

On the in-line motion of two spherical bubbles in a viscous fluid

By H. YUAN AND A. PROSPERETTI

Department of Mechanical Engineering, The Johns Hopkins University,
Baltimore, MD 21218, USA

The motion of two equal spherical bubbles moving along their line of centres in a viscous liquid is studied numerically in bispherical coordinates. The unsteady Navier–Stokes equations are solved using a mixed spectral/finite-difference scheme for Reynolds numbers up to 200. Free-slip conditions at the bubble surfaces are imposed, while the normal stress condition is replaced by the sphericity constraint under the assumption of small Weber number. The vorticity shed by the upstream bubble affects the drag on the trailing bubble in a very complex fashion that appears to be quite beyond the power of existing asymptotic analyses. The separation between two equal bubbles rising in line under the action of buoyancy is predicted to reach an equilibrium value dependent on the Reynolds number. This result is at variance with experiment. The explanation offered of this difference casts further doubt on the feasibility of a simplified simulation of bubbly liquid dynamics.

1. Introduction

In addition to its intrinsic fluid dynamic interest, the study of the interaction of two or more bodies in a flow is a necessary step in the derivation of averaged equations for multi-phase flows. Classic examples are the papers by Batchelor (1972) and Batchelor & Green (1972) in which results for two spheres at vanishing Reynolds number Re were used to study the sedimentation and effective viscosity of suspensions. Many other examples can be found in the literature. Here we are interested in the case of two bubbles at large Reynolds numbers where the interaction is mostly inertial.

For a dispersion of gas bubbles in a small-viscosity liquid, the vanishing of the shear stress at the bubble surfaces has the consequence that viscous effects only provide a correction of order $Re^{-1/2}$ to the basic potential flow. One may therefore try to construct a basically inviscid theory of bubbly liquids in which viscous effects are incorporated in an approximate way. Recent examples may be found in studies by Kok (1989), Sangani & Didwania (1993a, b), Kumaran & Koch (1993a, b), and van Wijngaarden (1993), in which the bubbles are treated as rigid stress-free spheres. For liquids like water and normal gravity, the bubble size range in which distortion of the spherical shape is small, of the order of 1 mm. Sangani & Didwania (1993b) included viscous effects by means of a dissipation function by setting, for the viscous force F_v^α acting on bubble α,

$$F_v^\alpha = \tfrac{1}{2}\nabla_{V^\alpha}\dot{E}_d, \tag{1.1}$$

where $\dot{E}_d$ is the instantaneous dissipation function approximately calculated from the potential flow and the gradient is taken with respect to the velocity of bubble α. Since $\dot{E}_d$ is bilinear in the bubble velocities, (1.1) is equivalent to a representation of the type

$$F_v^\alpha = \sum A_{\alpha\beta} V^\beta, \tag{1.2}$$

where $A_{\alpha\beta}$ is a matrix dependent only on the bubbles' configuration (Sangani & Didwania 1993*b*). For a single stress-free sphere at large *Re* it is well-known that this method gives the correct result in steady motion, namely

$$F_v = 12\pi\mu a V, \tag{1.3}$$

as first found by Levich (1962). Here μ is the liquid viscosity and a the sphere radius. The validity of this expression for unsteady motion is not obvious as, in principle, one might expect that the diffusive nature of viscous processes would introduce history-dependent terms in the drag law. As shown by Prosperetti (1977) for small-amplitude motion, and more recently by Kang & Leal (1988) for finite displacements, Levich's relation does nevertheless continue to hold with an accuracy of $O(Re^{-1/2})$. Based on the unsteady boundary-layer approximation, Chen (1974) reached a similar conclusion. More recently, Mei & Klausner (1992) studied the same problem in the frequency domain with the same results. In the studies of Kumaran & Koch and van Wijngaarden, (1.3) is used directly disregarding the effects of bubble–bubble interactions.

The validity of either approximation in the case of two or more bubbles is, however, unknown and this motivates the present study. At high Reynolds numbers the boundary layer is thin and the interaction is therefore maximized when a bubble is in the wake of another one. For this reason, and because the resulting axial symmetry considerably simplifies the analysis, we study two bubbles in motion in the direction of their line of centres. By the use of bispherical coordinates the physical domain is mapped onto a simple computational domain in which the vorticity/stream-function equations are solved by a mixed spectral and finite-difference method. We study the cases of motion with both imposed velocities and imposed forces, such as buoyancy.

Our results imply that the high-Reynolds-number limit in which the simplified asymptotic results hold is very high indeed, and possibly so high as to be of very limited practical interest. At Reynolds numbers as large as 200, corresponding approximately to a 0.8 mm diameter bubble rising in water, viscous effects beyond the Levich result are still quite significant and bubble–bubble interactions very strong. As a consequence, the theory of Harper (1970) for the rise of a chain of bubbles at large *Re* does not seem to have a useful range of applicability.

While numerical studies are available of the motion of one, two, or more no-slip rigid spheres (Tal, Lee & Sirignano 1984; Ramahandran *et al.* 1991), the problem studied here has not been considered previously other than in the paper by Harper (1970) mentioned before. The literature on single bubbles, on the other hand, is richer. In addition to the papers mentioned, one should include the first fully numerical study of a spherical bubble by Brabston & Keller (1975). Ryskin & Leal (1984*a*, *b*) considered the steady problem allowing for the deformation of the bubble and computed the drag coefficient as a function of the Reynolds and Weber numbers.

2. Formulation

We consider an incompressible viscous fluid occupying the domain exterior to two equal spheres of radius a translating in the direction of their line of centres. This is taken as the x-axis and is oriented from bubble 2 to bubble 1. If V_1, V_2 denote the velocities of the spheres, the distance d between their centres changes at the rate

$$\dot{d} = V_1 - V_2, \tag{2.1}$$

and the velocity of the midpoint of the segments joining the centres is

$$\dot{X} = \tfrac{1}{2}(V_1 + V_2). \tag{2.2}$$

We take this point as the origin of a cylindrical coordinate system (r, x, ϕ) and define bispherical coordinates (μ, η, ϕ) by

$$r = \frac{c \sin \eta}{\cosh(\mu_0 \mu) - \cos \eta}, \quad x = \frac{c \sinh(\mu_0 \mu)}{\cosh(\mu_0 \mu) - \cos \eta}, \tag{2.3}$$

where
$$c = (\tfrac{1}{4}d^2 - a^2)^{1/2}, \quad \mu_0 = \ln\left(\frac{c + \tfrac{1}{2}d}{a}\right). \tag{2.4}$$

The angular variable is the same in both systems. The metric coefficients are

$$h_\mu = \frac{c\mu_0}{\cosh(\mu_0 \mu) - \cos \eta}, \quad h_\eta = \frac{c}{\cosh(\mu_0 \mu) - \cos \eta}, \tag{2.5}$$

$$h_\phi = \frac{c \sin \eta}{\cosh(\mu_0 \mu) - \cos \eta}. \tag{2.6}$$

Owing to the motion of the bubbles, the coordinate transformation depends on time. In particular,

$$\dot{c} = \frac{d}{4c}(V_1 - V_2), \quad \dot{\mu}_0 = \frac{2\dot{c}}{d}, \tag{2.7}$$

and also, if we denote by $\dot{\mu}$, $\dot{\eta}$ the time derivatives of μ and η at constant field point x,

$$\begin{aligned} c\mu_0 \dot{\mu} &= \dot{c} \sinh(\mu_0 \mu) \cos \eta - \dot{X}[\cosh(\mu_0 \mu) \cos \eta - 1] - c\mu \dot{\mu}_0, \\ c\dot{\eta} &= \dot{c} \cosh(\mu_0 \mu) \sin \eta - \dot{X} \sinh(\mu_0 \mu) \sin \eta. \end{aligned} \right\} \tag{2.8}$$

The presence of axial symmetry suggests the use of a formulation in terms of the vorticity and the vector potential $e_\phi \psi$ or stream function $h_\phi \tilde{\psi}$. The two differ by the explicit inclusion of the metric coefficient in the latter quantity (see e.g. Gresho 1991). For the case of a single bubble in potential flow, in cylindrical coordinates, the stream function is given by $\tfrac{1}{2}Ur^2$ while the vector potential equals $\tfrac{1}{2}Ur$. The Fourier sine expansion of the vector potential thus only has one non-zero term, while that of the stream function has infinitely many terms. Our numerical evidence shows that this advantage of the vector potential carries over to the two-bubble case that we consider in the sense that the Fourier series for $\tilde{\psi}$ is found to converge more slowly than that for ψ. We therefore write

$$\boldsymbol{u} = \nabla \times (\psi \boldsymbol{e}_\phi), \tag{2.9}$$

so that the vorticity
$$\omega \boldsymbol{e}_\phi = \nabla \times \boldsymbol{u}, \tag{2.10}$$

is given by
$$\omega \boldsymbol{e}_\phi = \nabla \times \nabla \times (\psi \boldsymbol{e}_\phi). \tag{2.11}$$

Accounting for the time dependence of the coordinate system the vorticity equation is

$$\frac{\partial \omega}{\partial t} + \dot{\mu}\frac{\partial \omega}{\partial \mu} + \dot{\eta}\frac{\partial \omega}{\partial \eta} + (\boldsymbol{u} \cdot \nabla)\omega = \omega(\boldsymbol{e}_\phi \cdot \nabla)\boldsymbol{u} + \frac{2}{Re}\nabla^2 \omega. \tag{2.12}$$

Here and in the following we use quantities rendered non-dimensional with respect to the length a, velocity V, and pressure ρV^2. The choice of the fundamental velocity V

is problem-dependent and will be specified below for the different cases. The Reynolds number is based on the bubble diameter and is defined by

$$Re = 2aV/\nu, \tag{2.13}$$

with ν the kinematic viscosity.

The explicit expressions for (2.11) and (2.12) in bispherical coordinates are given in the Appendix. Here we use the more synthetic notation

$$\mathcal{L}_1 \psi - 2A(\eta)\,\omega = 0, \tag{2.14}$$

and

$$A(\eta)\,Re\frac{\partial \omega}{\partial t} + (\mathcal{L}_1 + Re\,\mathcal{L}_2)\,\omega = Re\,\mathcal{N}(\omega, \psi), \tag{2.15}$$

respectively, where $A = 2c^2(1 - \cos 2\eta)$, $\mathcal{L}_1$, $\mathcal{L}_2$ are linear operators, and $\mathcal{N}(\omega, \psi)$ denotes the bilinear term.

As explained in the Introduction our aim is to model bubbles and therefore we impose a condition of vanishing tangential stress at the surface of the spheres

$$\boldsymbol{\sigma} \times \boldsymbol{n}^\alpha|_{S^\alpha} = 0, \quad \alpha = 1, 2, \tag{2.16}$$

which, in terms of ψ, ω, may be compactly expressed as

$$\omega|_{S^\alpha} = \mathcal{F}^\alpha(\psi), \quad \alpha = 1, 2, \tag{2.17}$$

where $\mathcal{F}^{1,2}$ are linear operators given in the Appendix.

With the neglect of the deformation of the bubbles, the kinematic boundary condition is

$$(\boldsymbol{u} - \boldsymbol{V}^\alpha) \cdot \boldsymbol{n}^\alpha|_{S^\alpha} = 0, \quad \alpha = 1, 2, \tag{2.18}$$

which, in terms of ψ, may be written as

$$\psi|_{S^\alpha} = -\tfrac{1}{2}V^\alpha \frac{c \sin \eta}{\cosh \mu_0 - \cos \eta}, \quad \alpha = 1, 2. \tag{2.19}$$

Since we are going to neglect the gas inertia, the forces acting on each bubble must balance so that we have the integral constraint on the normal stresses

$$\int_{S^\alpha} \boldsymbol{\sigma} \cdot \boldsymbol{n}\,dS^\alpha = \boldsymbol{F}_\alpha, \quad \alpha = 1, 2, \tag{2.20}$$

where $\boldsymbol{F}_\alpha$ is the non-hydrodynamic force (e.g. buoyancy) acting on bubble α.

To impose these conditions the pressure on the bubble surfaces is needed. After the vorticity and vector potential have been calculated, this quantity can be obtained by integrating the η-component of the momentum equation along the bubble surfaces as done in Ryskin & Leal (1982). It is convenient to use a local spherical coordinate system (ϖ, θ, ϕ) centred at the centre of each bubble with θ measured from the direction of x positive. The dimensionless pressure is given by

$$p = p_0 - (u_\theta - V_\alpha \sin \theta)^2 + \dot{V}_\alpha(\cos \theta - 1) - \int_0^\theta \left[\frac{4}{Re}\left(\frac{\partial \omega}{\partial \varpi} + \omega\right) + 2\frac{\partial u_\theta}{\partial t} \right] d\theta, \tag{2.21}$$

where the index 0 denotes the stagnation-point value.

In general the effect of viscosity on the hydrodynamic force on a body is due not only to the viscous stress at the surface and to a viscous modification of the pressure, but also to a change of the entire flow pattern. Because of this circumstance, the identification of the 'viscous component' of the force is in general a somewhat ill-

defined question. However, at large Reynolds numbers and with free-slip boundary conditions, the flow structure in the inviscid and viscous cases is very similar (in particular, there is no separation) so that it is reasonable to *define*

$$F_v = F - F_{potential}.\qquad(2.22)$$

Here F is the x-component of the force given by (2.20) and $F_{potential}$ is calculated by solving (2.14) with $\omega = 0$ and using (2.10), also with $\omega = 0$. This latter calculation could of course be done analytically. However, the final result is quite cumbersome and in the end it proved more practical to proceed numerically as the same code can be used. The drag coefficient discussed below is defined by

$$C_D = \frac{2}{\pi}F_v.\qquad(2.23)$$

For the time-dependent problems to be considered below we take the initial condition to correspond to purely potential flow,

$$\omega(\mu, \eta, 0) = 0.\qquad(2.24)$$

This would be applicable, for example, to an impulsively started motion. A discussion of initial conditions of this type is given by Gresho (1991).

We will first solve the problem in which the velocity of the bubbles is precribed (§3). The procedure will then be extended to study the motion of the bubbles under the action of prescribed forces (§5).

3. Solution procedure

For prescribed bubble velocities, the equations to be solved are (2.14) and (2.15) subject to the boundary conditions (2.17) and (2.19).

To solve the field equations ω and ψ are expanded in a Fourier sine series in the η-direction truncated at some finite number of terms N:

$$\left.\begin{array}{l} \omega(\mu, \eta, t) = \displaystyle\sum_{k=1}^{N} \hat{\omega}_k(\mu, t) \sin(k\eta), \\[2mm] \psi(\mu, \eta, t) = \displaystyle\sum_{k=1}^{N} \hat{\psi}_k(\mu, t) \sin(k\eta). \end{array}\right\}\qquad(3.1)$$

Upon substitution into (2.14) and (2.15) and application of the standard Garlerkin method (see e.g. Canuto *et al.* 1988) we find

$$\sum_{l=1}^{N} (\mathrm{L}^1_{k,l}\hat{\psi}_l - 2A_{k,l}\hat{\omega}_l) = 0, \quad k = 1, 2, \ldots, N,\qquad(3.2)$$

$$\sum_{l=1}^{N}\left[Re\, A_{k,l}\frac{\mathrm{d}\hat{\omega}_l}{\mathrm{d}t} + (\mathrm{L}^1_{k,l} + Re\,\mathrm{L}^2_{k,l})\right]\hat{\omega}_l = Re\, N_k(\mu), \quad k = 1, 2, \ldots, N,\qquad(3.3)$$

where $N_k(\mu)$ indicates a convolution product and $A_{k,l}$ a matrix. The operators $\mathrm{L}^1_{k,l}, \mathrm{L}^2_{k,l}$ involve differentiation with respect to μ. The explicit expressions for all these quantities are given in the Appendix. The boundary conditions must also be expanded in a Fourier sine series. This can be done either numerically by using the FFT, or analytically as described in the Appendix.

The use of a spectral expansion in the μ-direction, although of course possible, is rather involved owing to the presence of the metric coefficients. We choose instead a

finite-difference approach which has the advantage of leading to a block tri-diagonal matrix with blocks of dimension N. All the μ-derivatives are discretized using standard central differences.

Time integration is carried out by the backward Euler sheme with iterative solution of the implicit equations. At each time step the algebraic problem to be solved has the structure

$$\sum_{j=1}^{M}\sum_{l=1}^{N} L^1_{i,k;j,l}\hat{\psi}^{n+1}_{j,l} = 2\sum_{l=1}^{N} A_{k,l}\hat{\omega}^{n+1}_{i,l}, \quad k=1,2,\dots,N, \quad i=1,2,\dots,M, \quad (3.4)$$

$$\sum_{j=1}^{M}\sum_{l=1}^{N}\left[Re\frac{A_{k,l}}{\Delta t}\delta_{i,j}+(L^1_{i,k;j,l}+Re\,L^2_{i,k;j,l})\right]\hat{\omega}^{n+1}_{j,l} = Re\,N^{n+1}_{i,k}+\sum_{l=1}^{N} Re\frac{A_{k,l}}{\Delta t}\hat{\omega}^{n}_{i,l},$$

$$k=1,2,\dots,N, \quad i=1,2,\dots,M. \quad (3.5)$$

The matrices $L^1_{i,k;j,l}, L^2_{i,k;j,l}$ arise from the discretization of the differential operators $L^1_{k,l}, L^2_{k,l}$ and $N^{n+1}_{i,k}$ depends on $\hat{\psi}^{n+1}_{i,k}, \hat{\omega}^{n+1}_{i,k}$. Detailed expressions for all these quantities are given in the Appendix.

The iterative procedure is as follows. We first solve (3.4) subject to the kinematic boundary condition (2.19) using, on the right-hand side, the most recent value of the vorticity distribution. With the resulting updated value of ψ, the vorticity equation (3.5) is solved subject to the dynamic boundary condition (2.16). The nonlinear term $N_{i,k}$ is calculated using a $2N$-point FFT from the results of the previous iteration. Each iteration requires two block-tridiagonal matrix inversions. The procedure is continued until convergence, which is monitored through the computed hydrodynamic forces. In the early stages of this work we kept track of the maximum norm of the difference between the actual field values at each iteration, but we found that the force criterion is simpler and just as accurate. The iterations were stopped when successive force values differed by about 10^{-7}.

After each iteration, the pressure on the bubble surface is obtained by integrating the η-component of the momentum equation according to (2.21), and the drag is then found by integrating the normal stress around the bubbles. In this calculation analytical expressions (given in the Appendix) are used to express in (ϖ,θ)-coordinates the velocity components given in terms of (μ,η)-coordinates.

The number N of terms in the spectral expansion and M of nodes is dependent on both the Reynolds number and the separation between the bubbles. The Reynolds-number dependence arises from the boundary-layer-type behaviour of the solution, while the separation dependence is due to the grid clustering occurring in bispherical coordinates shown in figure 1. When the bubbles are very close more nodes are required to ensure adequate resolution ahead of, and behind, the bubble pair. In addition there is a dependence on the duration of the simulation as the wake becomes very long for large times, even though the drag coefficients have reached a steady value. In the calculation we used between 32 and 64 terms in the Fourier sine expansion for both ω and ψ and 300 finite-difference points. Standard convergence tests showed that, for the present results, this resolution was adequate for Re up to 200 and centre-to-centre separations of three times the radius or larger. Since the stream function and drag coefficients are obtained from the vorticity essentially by integration, one expects that numerical inaccuracies would first manifest themselves in the results for ω. Indeed, we found that, when M, N are too small, the calculated vorticity field presents oscillations in the nearly irrotational region, while the other quantities are nearly unchanged.
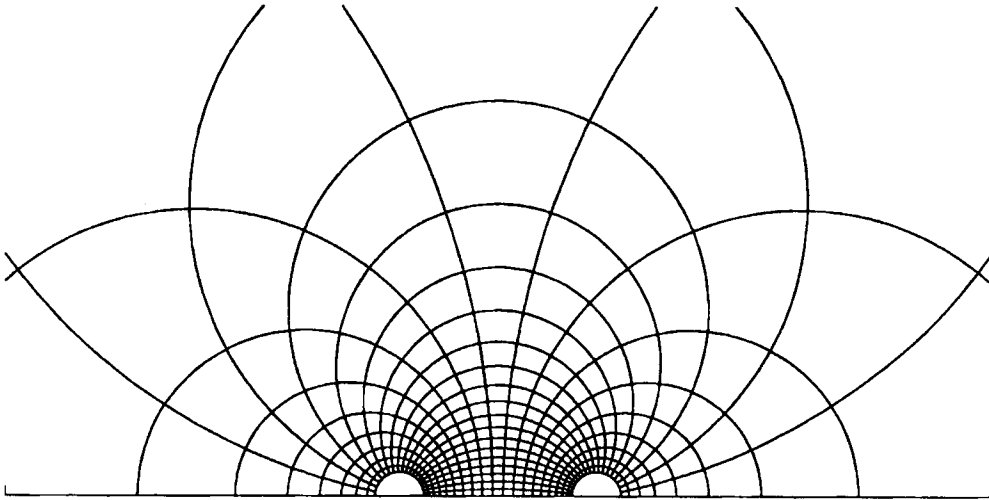
FIGURE 1. Portion of the computational grid for a bubble separation 8 times the radius. The actual computational domain is the entire space. Typically between 10 and 25 as many grid lines are used in the computations.

To test the accuracy of the computation, we let the separation between the bubbles be very large (say 100 radii) so that their interaction can be neglected. The drag coefficients calculated for this case were within 2.5% of the results for single spherical bubbles of Ryskin & Leal (1984 *a*).

4. Results – prescribed velocities

In this section, we will present some results for the case in which the bubbles move with equal imposed velocity V. Although this is a somewhat artificial situation, it is useful to illustrate the development of the flow field and the mechanisms influencing the drag forces.

We consider the steady case first. Figures 2(a) and 2(b) show the calculated steady drag (dashed lines) on the leading and trailing bubble, respectively, as a function of the separation d between the centres for several Reynolds numbers. The solid line in these figures is the dissipation-function prediction according to (1.1) and shows a much smaller range of variation than the full viscous results indicated by the dashed lines and corresponding, in ascending order, to $Re = 20, 50, 100, 200$. The reason is that the drag calculated from the dissipation function method depends on d only through the dependence of the potential on this quantity. Asymptotically this dependence is proportional to $(a/d)^3$ and is therefore relatively weak even at close separations. In a viscous fluid, on the other hand, the wake and other interaction mechanisms have a considerably longer range and produce very strong effects, as these figures demonstrate. Furthermore, for two bubbles moving with the same velocity, the dissipation method gives identical drags due to the time-reversal invariance of potential flow, while the fact that the trailing bubble is immersed in the wake of the leading one leads to markedly different results at finite Reynolds numbers. In the case of the leading bubble, the drag increase with separation predicted by the dissipation-function method occurs only for sufficiently large Reynolds numbers and separations. For smaller separations, the drag is actually a decreasing function of d. This feature may be explained by noting that, for an isolated bubble, the wake is thin so that the pressure recovers substantially over the
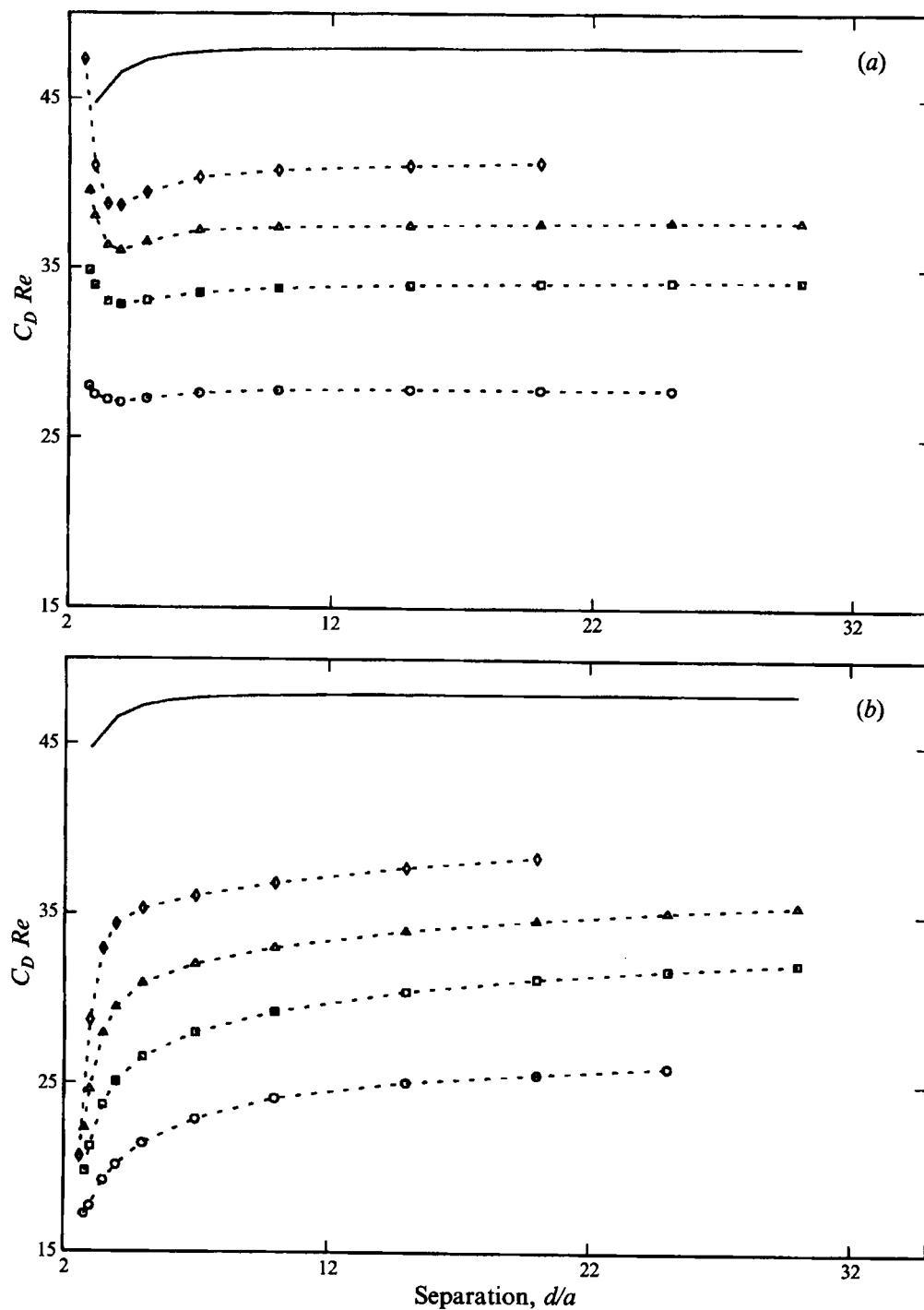
FIGURE 2. Steady drag on (*a*) the leading bubble, and (*b*) the trailing bubble, as a function of the centre-to-centre separation. The dashed lines, in ascending order, are for $Re = 20$, 50, 100 and 200. The solid line is the dissipation method prediction.
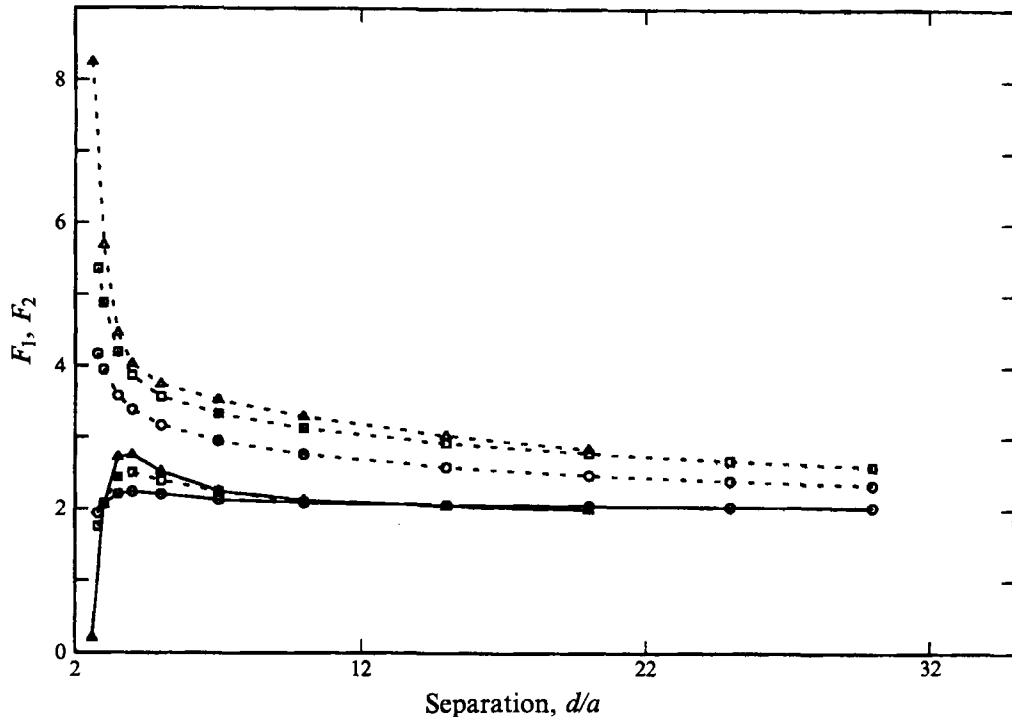
FIGURE 3. Correction factor F to the dissipation function drag defined in (4.1) as a function of the centre-to-centre distance for several values of the Reynolds number. The solid lines are for the leading bubble and the dashed lines for the trailing bubble. $\triangle$, $Re = 200$; $\square$, $Re = 100$; $\bigcirc$, $Re = 50$.

rear hemisphere. The proximity of a second bubble prevents this recovery and hence causes the drag to increase. The drag on the second bubble, on the other hand, increases monotonically due to the shielding effect of the leading bubble at small separations. This strong rise at small d is sufficient to offset the decline on the first bubble so that the average drag is monotonic.

It is well known that, for a single bubble, a better value than Levich's for the drag coefficient is given by (Moore 1963)

$$C_D = \frac{48}{Re}\left(1 - \frac{F}{Re^{1/2}}\right), \qquad (4.1)$$

with $F \approx 2.211$. We have tried to fit the numerical results of figure 2(a) with an expression of this type and found excellent results for $Re \geqslant 50$. From such a fit we can also obtain an estimate of the quantity $F(d/a)$ as a function of the separation between the bubbles. These results are shown in figure 3 by the solid lines which refer to different values of Re. At the higher separations and Reynolds numbers the curves converge, which supports an expression of the form (4.1) for the leading-order correction. Furthermore, the convergence of F to a value very close to 2.2 with increasing Reynolds number and separation is in agreement with the single-bubble results. The dependence upon Re at small separations indicates that (4.1) is inapplicable in this range. It is interesting and perhaps rather disappointing to see in figure 2(a) that the dissipation result gives an error of the order of 20% even for $Re = 200$.

A similar procedure applied to the results of figure 2(b) for the second bubble gives the results shown by the dashed lines in figure 3. Evidently, for the trailing bubble, a
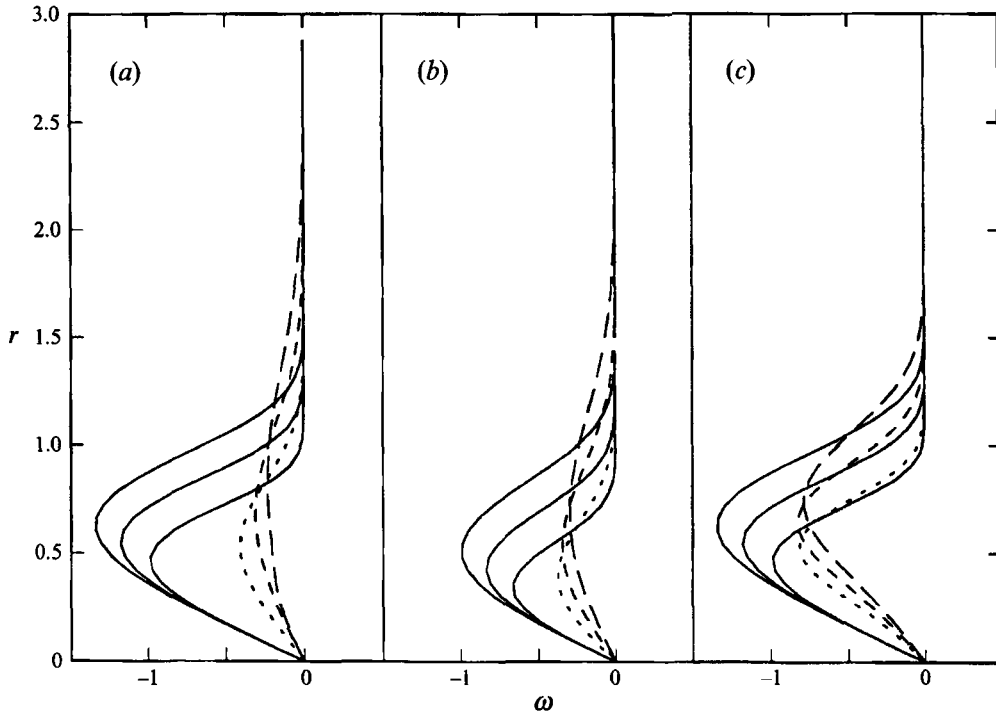
FIGURE 4. Vorticity distribution in three planes perpendicular to the axis of symmetry according to the present computations for $Re = 100$ (long dashes), 200 (medium dashes), and 500 (short dashes) and Harper's theory (solid lines, with Re decreasing from left to right). (a) The vorticity in a plane 0.16 radii ahead of the trailing bubble's front stagnation point, (b) in the plane of symmetry of the two bubbles, and (c) 0.16 radii behind the rear stagnation point of the leading bubble.

much greater separation is needed before (4.1) becomes applicable. As the distance between the bubble increases further, F for the second bubble must evidently tend asymptotically to the single-bubble value 2.2. The figure suggests that this would only occur at very large separations indeed. These results are in quantitative disagreement with the analysis of Harper (1970), who gave a formula similar to (4.1) with $F = 4.345$. It seems that the difference arises due to the approximations that he introduced for the vorticity field. To substantiate this diagnosis we show in figure 4 the vorticity distribution in three planes normal to the symmetry axis for $Re = 100$, 200 and 500. Here the bubble centres are separated by 8 radii and the planes are, from right to left, 0.16 units behind the rear stagnation point of the leading bubble, at the midpoint between the centres, and 0.16 units upstream of the front stagnation point of the trailing bubble. The solid lines are Harper's vorticity distributions as obtained from his equation (3.8), and the broken lines are the present computed results. It is seen that, for $Re = 500$, Harper's and the numerical results are fairly close, especially in the outer part of the wake. Closer to the axis of symmetry, however, Harper's vorticity is considerably stronger than the present one owing to his inadequate resolution of the flow near the rear stagnation point. This error is much greater for $Re = 100$ and 200. Downstream of this region the numerical results indicate, even for $Re = 500$, a strong diffusion of vorticity that is completely neglected by Harper. The comparison seems to suggest that Harper's and the present results approach each other as Re increases, but at a very slow rate. Thus it would seem unlikely that a realizable physical situation can
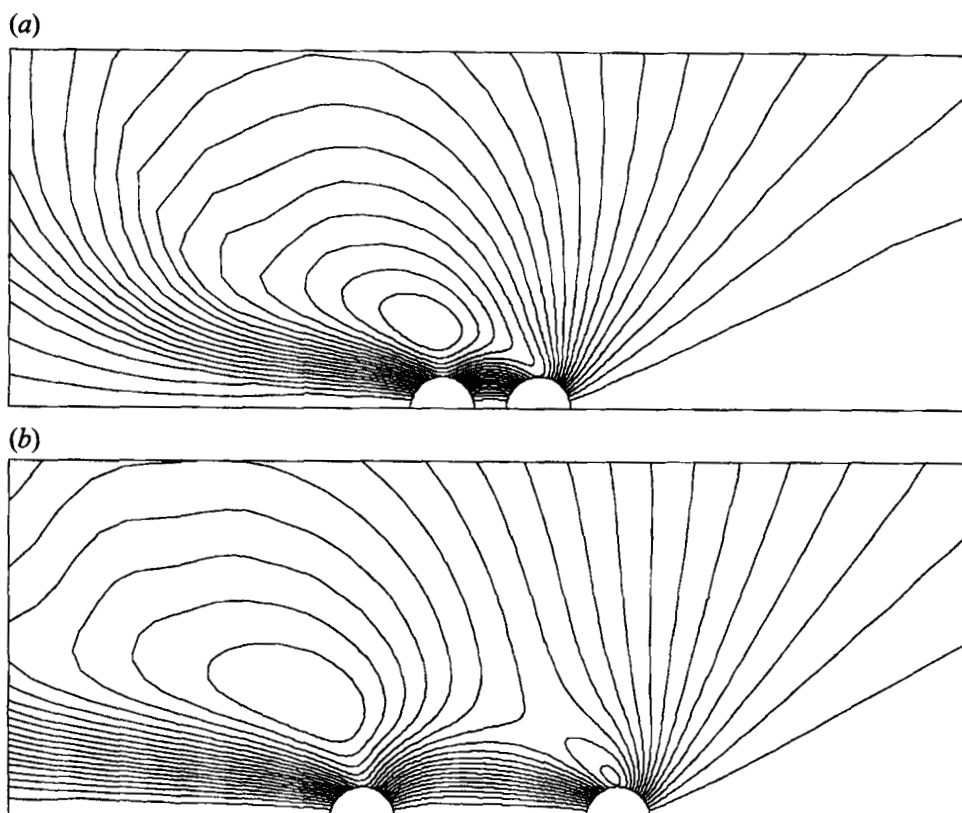
(a)

(b)

FIGURE 5. Streamlines of the relative flow in the rest frame of the bubbles at $Re = 20$ at a centre-to-centre separation of (a) 3 and (b) 8 radii. The stream function of the disturbance flow vanishes on the axis. Contours are separated by 0.4 dimensionless units.

be found in which the Weber number is small enough for the bubbles to remain appreciably spherical and the Reynolds number large enough for Harper's first-order boundary-layer theory to give accurate results.

Another approximation scheme to estimate the drag on the trailing bubble could be to use the same drag coefficient as for the leading bubble but with a relative velocity diminished by the wake effect. For this approximation to be valid the wake of the leading bubble must have had time to diffuse by a distance of the order of one bubble radius, which requires a separation d/a of the order of the Reynolds number. For these very large separations our numerical method is not very accurate but, on the other hand, since the correction to the drag obtained in this way is of the order of a/d, its magnitude is expected to be very small.

Figures 5 and 6 show the streamlines of the relative flow in the rest frame of the bubbles for $Re = 20$ and 200 at two separations, $d/a = 3$ and 8. For the higher-Re example of figure 6 the potential-flow streamlines are also shown, by the dashes, and figures $6(a)$(ii) and $6(b)$(ii) are enlargements of the flow near the spheres. The large difference between the viscous and inviscid flow fields even at this relatively high Re is in agreement with the drag results shown before.

We now turn to the unsteady problem and consider the evolution of the flow and of the drag for the case in which the motion starts impulsively at $t = 0$ with unit dimensionless velocity. The initial condition is potential flow.
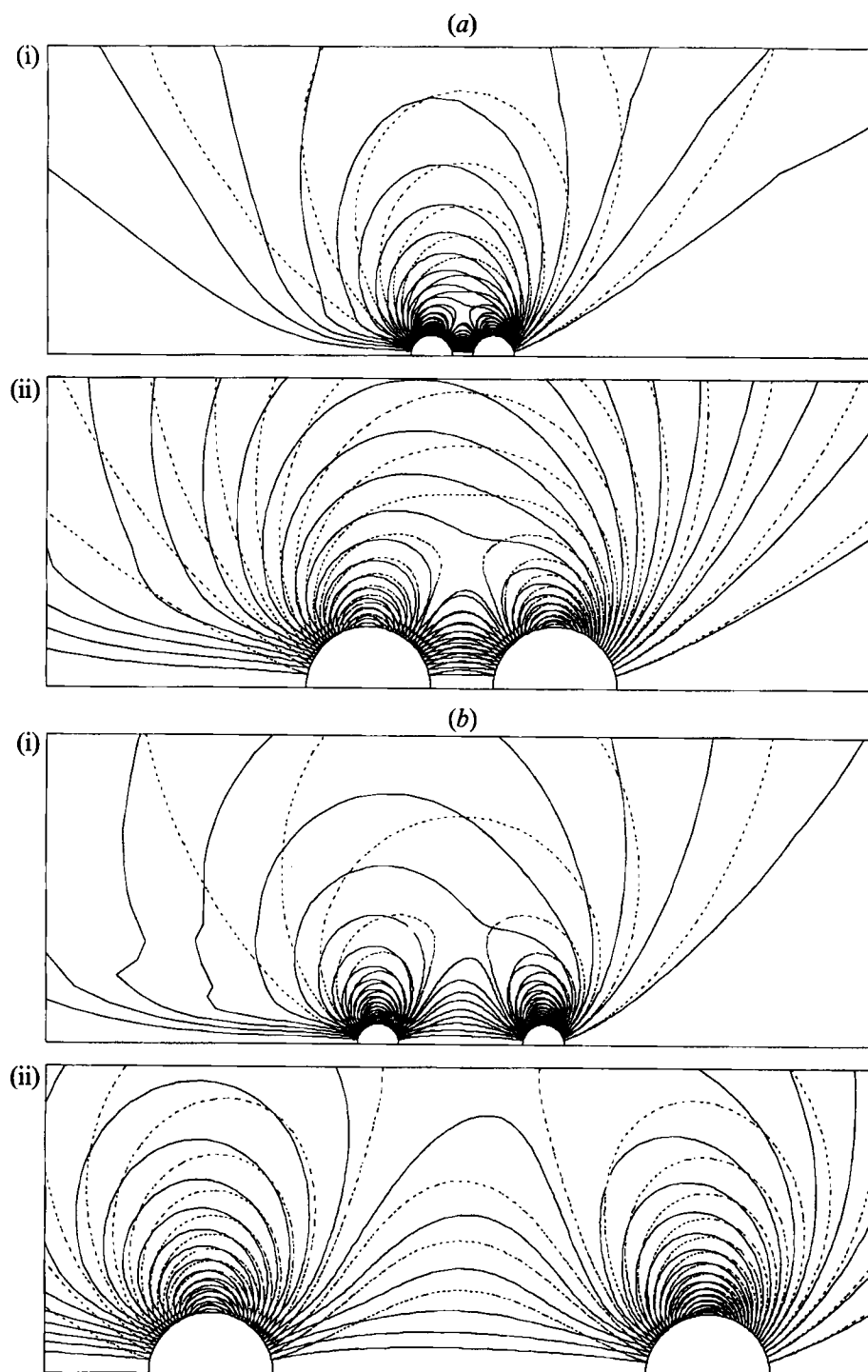
FIGURE 6. Streamlines of the relative flow in the rest frame of the bubbles at $Re = 200$ at a separation of 3 radii in (*a*) and 8 radii in (*b*). Panel (ii) shows detail of the flow near the bubbles. The dashed lines are the potential flow solution. The stream function of the disturbance flow vanishes on the axis. Contours are separated by 0.25 dimensionless units.
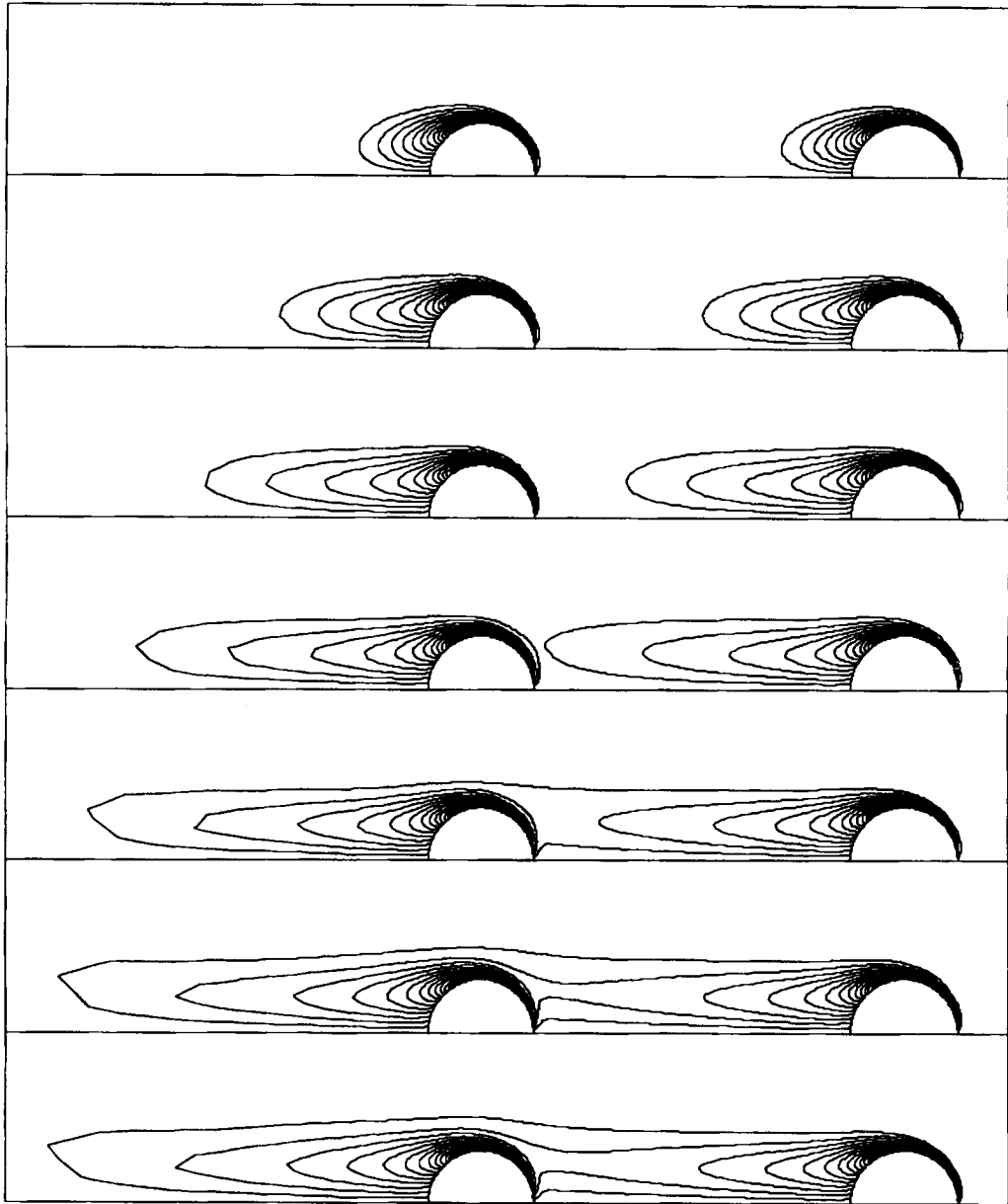
FIGURE 7. Transient evolution of the iso-vorticity contours after the impulsive motion of two bubbles with $Re = 100$ and a centre-to-centre distance of 8 radii. From top to bottom the panels are at dimensionless times equal to 2, 4, 6, 8, 10, 12 and 14. The outermost contour corresponds to $\omega = 0.2$ and adjacent contours differ by 0.2 units.

The first example is for a distance between bubble centres of 4 diameters with $Re = 100$. Figure 7 shows the time evolution of the iso-vorticity contours. The requirement of zero tangential stress causes vorticity to be generated at the bubble surfaces, after which it is convected downstream, forming a wake behind each bubble. Up to a dimensionless time $t_* = Vt/a \approx 8$, at which the wake of the first bubble reaches the second one, the vorticity fields around the two bubbles are almost the same. After $t_* = 8$ the wake of the first bubble strongly influences the flow structure around the
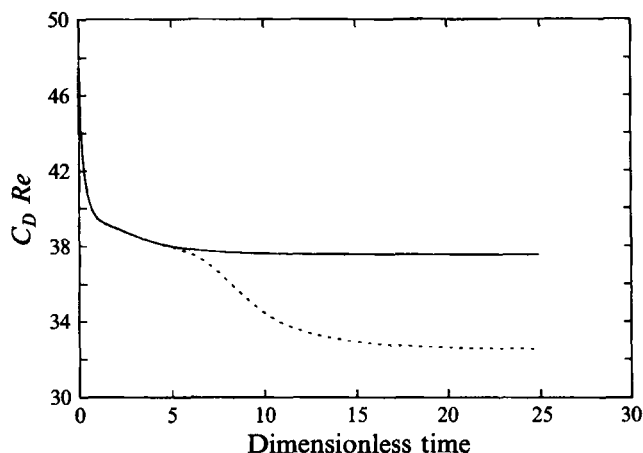
FIGURE 8. Time history of the drag on the leading (solid line) and trailing bubble for the case of figure 7.

second one but, owing to the dominance of convection, the leading bubble itself is little affected.

The effect of this flow development on the drag forces on the bubbles can be followed in figure 8 which shows the product of the drag coeffiient C_D and the Reynolds number as a function of time. As the flow initially is nearly potential and the bubbles are sufficiently far apart not to interact significantly other than through the wake, the initial value of $C_D Re$ is close to 48, in agreement with Chen's (1974) unsteady boundary-layer analysis of a single bubble. As the vorticity field develops, both drags rapidly decrease but remain nevertheless very close until the wake of the first bubble reaches the second one. At this point the drag in the trailing bubble falls sharply while that on the leading one remains essentially constant at $C_D Re \approx 37$. Shortly thereafter the drag on the second bubble also stabilizes at a value $C_D Re \approx 33$, significantly lower than that on the first bubble. Since potential flow does not include history effects the time dependence of the drag forces shown in this figure cannot possibly be accounted for by the dissipation-function method.

The time evolution is similar for other separations, but an interesting new feature appears at higher Reynolds numbers as shown in figures 9(*a*) and 9(*b*) where the drag history for the two bubbles is portrayed for several values of *d*. All the curves initially fall rather rapidly and reach a minimum or near-minimum close to $t_* = 2$, after which they show a tendency to rise and then to fall again toward a steady value (that in the case of the trailing sphere is modified once the wake of the leading one reaches it). The qualitative similarity of the trends and the closeness of the timescales suggest that these features are not due to the interaction, but are characteristic of the flow about each bubble. A possible interpretation is the following. Right after the initiation of the motion, the flow is very nearly potential and the drag is only due to the skin friction. With time, a viscous boundary layer forms and thickens, the velocity gradients relax, and the drag falls. Simultaneously, however, the fluid near the rear stagnation point starts moving with the body and so the pressure, that was high there in the initial quasi-potential flow, starts falling. The consequence is a tendency for the drag to increase. This state of affairs, however, is a temporary one as the vorticity distribution continues to evolve in the wake and to affect, via the Biot–Savart law, the velocity at the surface of the body. In support of this interpretation we note that the part of the argument
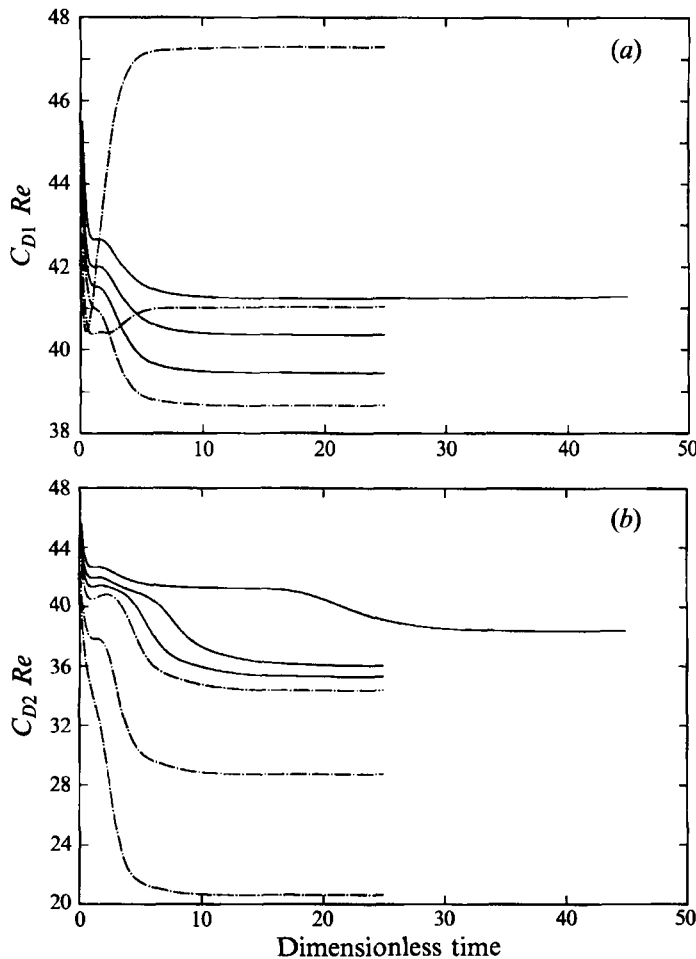
FIGURE 9. (a) Time history of the drag on the leading bubble at $Re = 200$ and different centre-to-centre separations. The broken lines, in descending order, are for $d/a = 2.6, 3, 4$. The solid lines, in ascending order, are for $d/a = 5, 7$ and 20. (b) As (a) but for the trailing bubble. The lines are, in ascending order, for $d/a = 2.6, 3, 4, 5, 7$ and 20. Note the difference between (a) and (b) in the vertical scales.

given to explain the drag rise is based on a Bernoulli effect that would be much smaller at lower Reynolds numbers, in agreement with the numerical results. Furthermore, the drag rise in the case of the smallest separation $d/a = 2.6$ is very large, as one would expect from the fact that the fluid between the spheres must acquire nearly the spheres' velocity in this case. The role of the wake development in the final adjustment of the drag is implied by the relatively long timescale over which it occurs.

Under the action of an imposed force, if the drag coefficients on the two bubbles are different, their distance will also change with time. The previous results show that the steady drag on the trailing bubble is always less than that on the leading bubble. The reverse is true, however, for the potential interaction. To show these features quantitatively we present in figures 10(a) and 10(b) graphs of $Re(C_{D1} - C_{D2})$ (solid line) and $Re(C_{p2} - C_{p1})$ (dashed line). Here C_p is the force coefficient for the potential flow component of the force, defined similarly to (2.23). Since this interaction leads to a repulsive force approximately inversely proportional to the fourth power of the
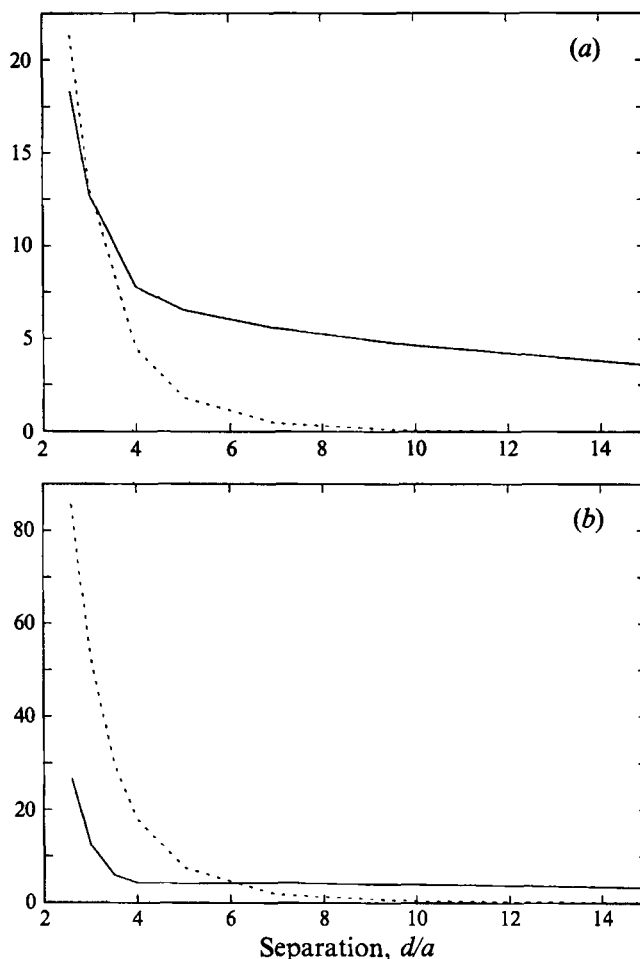
FIGURE 10. The solid line shows $Re(C_{D1} - C_{D2})$ as a function of the centre-to-centre distance. The dashed line is $Re(C_{p2} - C_{p1})$. The Reynolds number is 50 in (a) and 200 in (b). Note that the curves intersect at a point which corresponds to a stable separation between the bubbles.

separation (Harper 1970), the order of the terms has been reversed. The interesting point about these results is that the two curves cross, which implies an equilibrium distance at which the total hydrodynamic forces on each bubble are equal. It is clear that this situation corresponds to a stable equilibrium with respect to displacements in the direction of the line of centres. Indeed, if the bubbles get closer, the potential repulsive interaction would dominate and push them apart again while, if the separation were to increase, the viscous drag on the trailing bubble would fall and it would tend to catch up with the leading one. The implications of this will be discussed in the next section.

We show in figure 11 the computed equilibrium distances D_e for $Re = 50$, 100, and 200. The three results lie remarkably close to the straight line

$$D_e = 4.40 \log_{10} Re - 4.38. \tag{4.2}$$

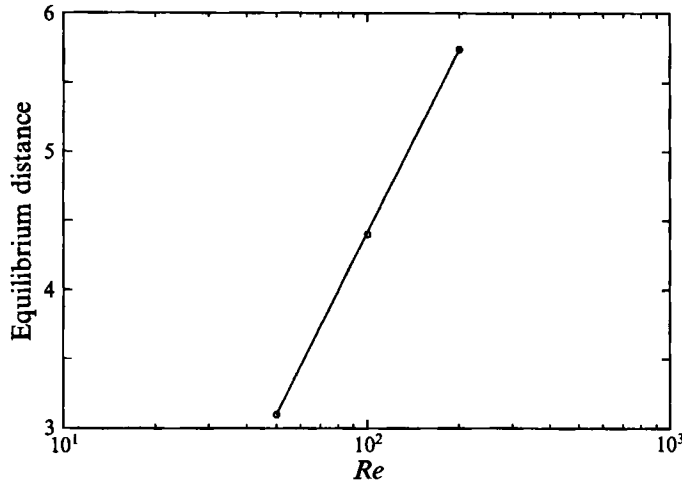For $Re = 20$, D_e is approximately 2.6 and is too small to be computed reliably by our method.

FIGURE 11. Equilibrium separation between two bubbles as a function of the Reynolds number.

5. Buoyant rise of two bubbles

We now describe some results for the more realistic case in which the external forces, rather than the velocities, are prescribed. The motion of the bubbles must now be found in such a way that the total instantaneous force on them vanishes according to (2.20). In this equation the prescribed non-hydrodynamic force F^α is taken as due to buoyancy, so that the flow field can be computed ignoring the body force. An equivalent alternative of course would be to set $F^\alpha = 0$ and to retain the body force in the Navier–Stokes equations.

As in the previous case, in defining the viscous force on the bubbles, the potential force must be identified and subtracted. For this purpose we use the results of Lamb (1932, art. 138) to write

$$\left.\begin{aligned}
\frac{d}{dt}(LV^1 - MV^2) - \frac{1}{2}\left[\frac{dL}{dd}(V^1)^2 - 2\frac{dM}{dd}V^1V^2 + \frac{dL}{dd}(V^2)^2\right] = F^1 - F_v^1, \\
\frac{d}{dt}(LV^2 - MV^1) + \frac{1}{2}\left[\frac{dL}{dd}(V^1)^2 - 2\frac{dM}{dd}V^1V^2 + \frac{dL}{dd}(V^2)^2\right] = F^2 - F_v^2,
\end{aligned}\right\} \quad (5.1)$$

where $F^{1,2}$ are the buoyancy forces and $F_v^{1,2}$ are defined by (2.22). L and M are added-mass coefficients depending on bubble radius and separation. When the spheres have the same radius and are well separated, $a \ll d$, they are given by (Lamb 1932, art. 98)

$$L = \tfrac{2}{3}\pi\rho a^3\left[1 + \frac{3}{[(d/a)^2 - 1]^3} + \frac{3}{[(d/a)^4 - 3(d/a)^2 + 1]^3} + \cdots\right], \quad (5.2)$$

$$M = 2\pi\rho a^3\left(\frac{a}{d}\right)^3\left[1 + \frac{1}{[(d/a)^2 - 2]^3} + \frac{1}{[(d/a)^4 - 4(d/a)^2 + 3]^3} + \cdots\right]. \quad (5.3)$$

In the present calculations the minimum value of d/a is 2.6 and the last terms retained in these expressions are smaller than 2×10^{-4}. The characteristic velocity used in the present problem is the velocity of rise of a pair of bubbles at the equilibrium distance found at the end of the previous section.

Since the viscous force acting on the bubbles depends on their velocity and separation, and since these quantities are themselves to be determined at each time step, the equations of motion (5.1) are implicit. To solve them we first discretize the
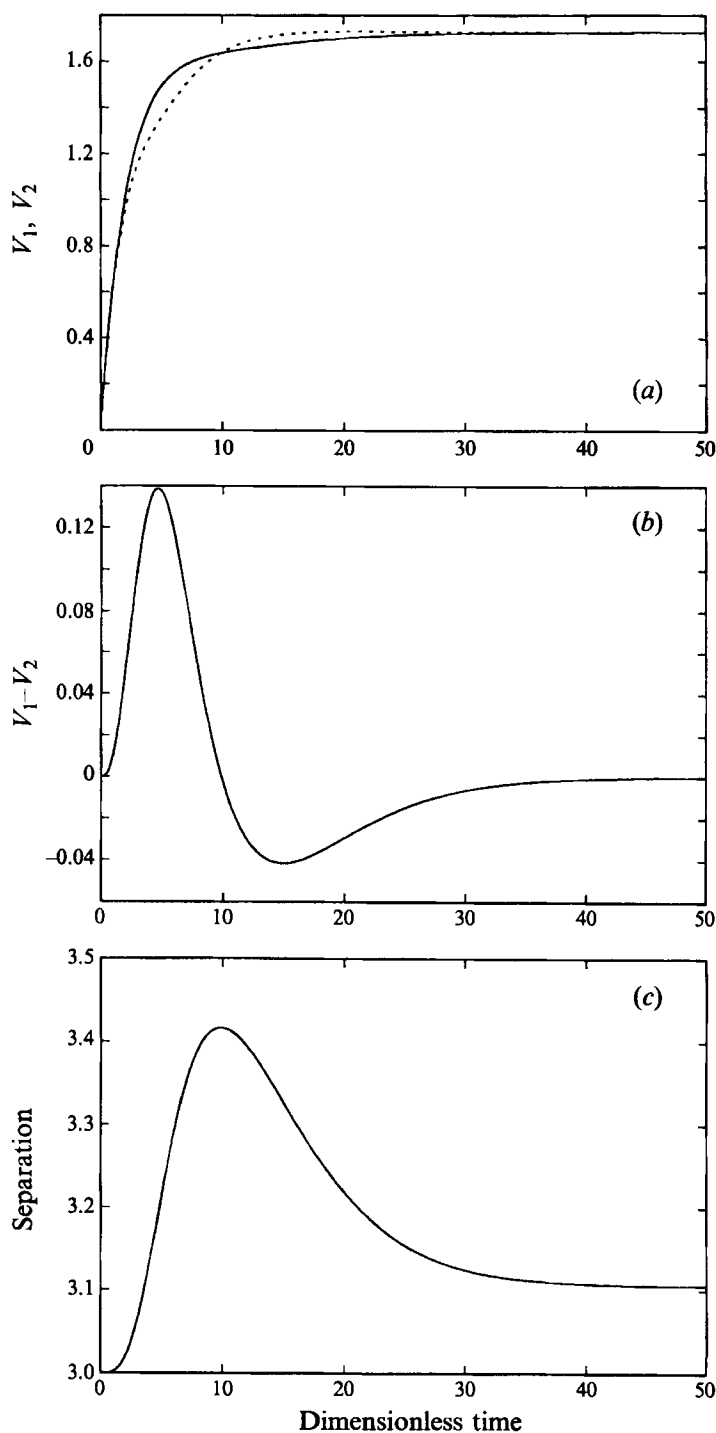
FIGURE 12. History of (*a*) the individual velocities, (solid line, leading bubble, dashed line, trailing bubble), (*b*) relative velocity, and (*c*) centre-to-centre separation, for two bubbles ascending under the action of a fixed force. The initial centre-to-centre separation is 3 radii and the Reynolds number 50.
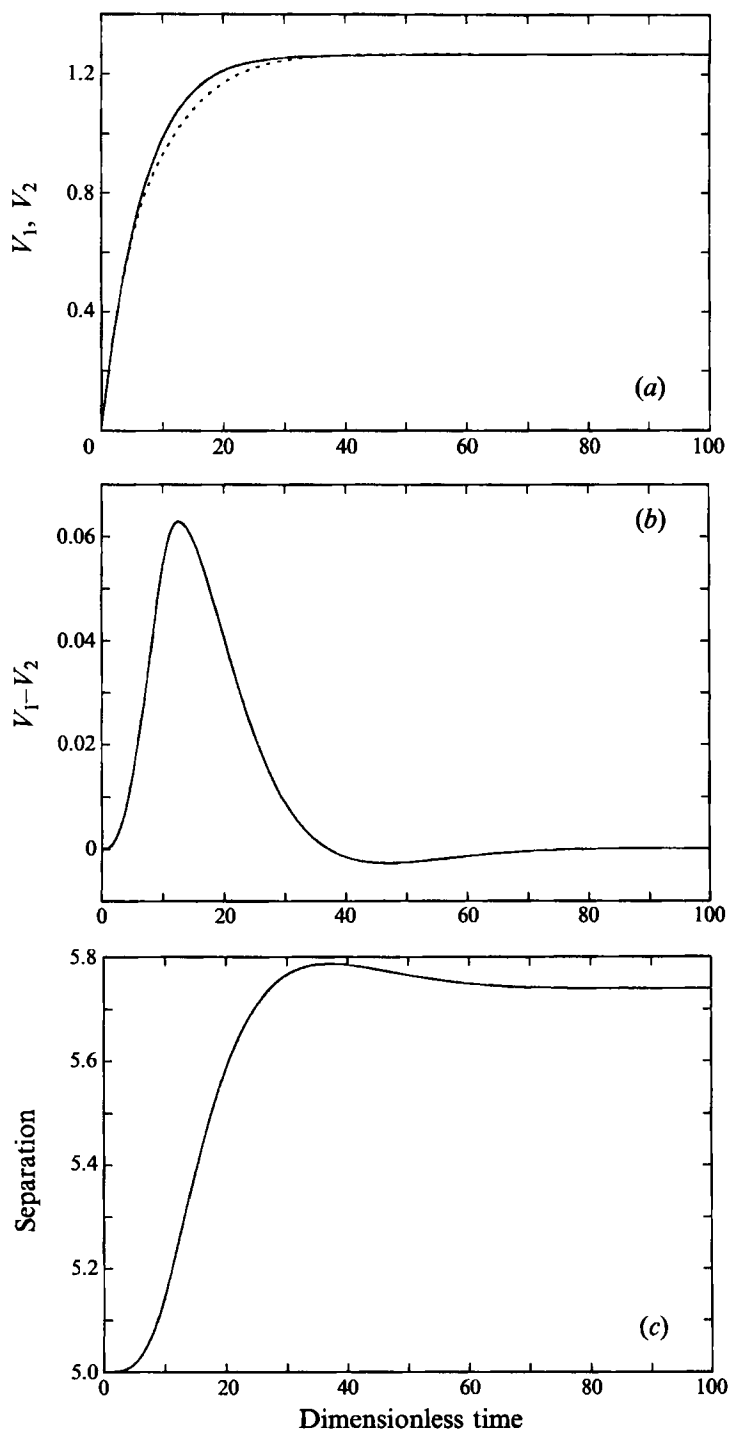
FIGURE 13. As figure 12 but the initial centre-to-centre separation is 5 radii and the Reynolds number 200.
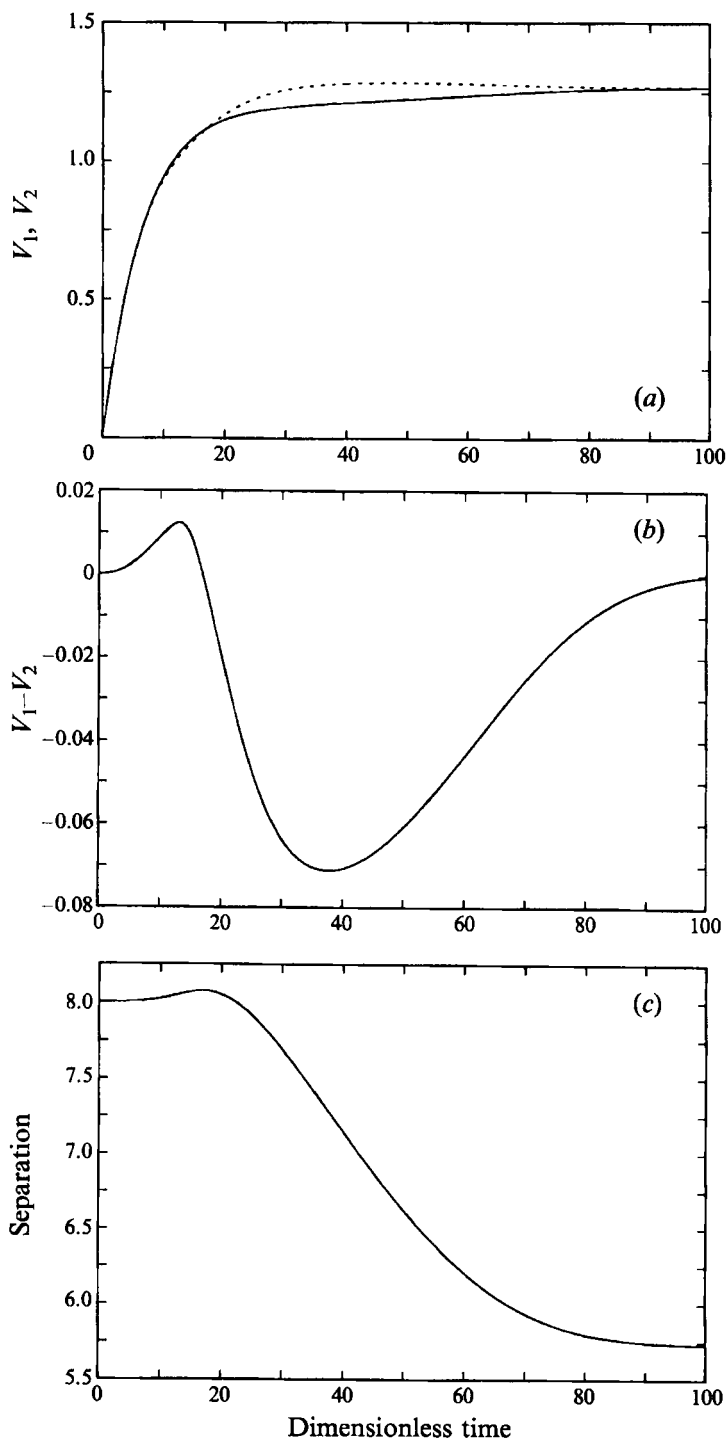
FIGURE 14. As figure 12 but the initial centre-to-centre separation is 8 radii and the Reynolds number 200.

time derivatives by the backward Euler scheme. Given then an initial guess for the bubbles' velocity and position, the flow field is determined and the viscous forces calculated by using the method of the previous section. The equation of motion (5.1) is then integrated to get a new estimate of velocities and positions, and so on to convergence. The convergence rate chiefly depends on the time step. For the typical value $\Delta t = 0.1$ approximately 5 iterations are required for a tolerance of 10^{-6}.

We show some examples in figures 12–14. To interpret these results it is necessary to recall from the last section the fact that, at any Reynolds number, a separation exists at which the mutual forces between the bubbles balance. Hence it is expected that, whatever the initial separation between the bubbles, their distance will eventually reach the equilibrium value such that the forces on them are equal and they rise at the same velocity. This behaviour is indeed encountered in the calculations. For $Re = 50$ the equilibrium separation is approximately $d/a \approx 3.10$. Figures 12 and 13 show the velocity and separation histories for two bubbles separated initially by $d/a = 3$ and 8 for $Re = 50$. In the first case, initially, the trailing bubble is subject only to the potential force and its velocity is smaller than that of the leading bubble. When the leading wake develops, however, the drag falls and the velocity overshoots that of the leading bubble. The separation decreases until the repulsive force dominates and pushes the trailing bubble back to its equilibrium distance. A similar behaviour can be seen in figure 14, for $Re = 200$ and $d/a = 5$. The equilibrium distance is in this case $d/a \approx 5.75$.

6. Conclusions

The present results have revealed that very strong viscous effects influence the interaction of two bubbles moving in the direction of their line of centres. The available high-Reynolds-number limiting results are very inaccurate even at $Re = 200$. At still larger values of Re, the Weber number increases and the assumption of sphericity becomes unjustified. These circumstances render the asymptotic study of Harper (1970) of bubbles rising in line of little relevance for the situations considered here and, presumably, for most of those encountered in practice as well.

The transport and diffusion of vorticity affects very strongly the interaction between the bubbles, introducing history effects that cannot possibly be simulated from the dissipation function based on potential flow as in (1.1). The implications of this conclusion for the simulation of bubbly liquids along the lines of several recent papers (Sangani & Didwania 1993 a, b; Kumaran & Koch 1993 a, b; van Wijngaarden 1993) are unclear. We have studied here the configuration that maximizes the viscous interaction. In view of the relatively small extent of the viscous region, (1.1) is expected to do a much better job at describing viscous forces in most other configurations. If, as argued by Kumaran & Koch (1993a), the effect of the lift force is such as to repel a bubble away from the wake of another bubble, one would conclude that the situation studied here occurs with very low probability and therefore the error incurred in modelling it incorrectly is small. On the other hand, Kumaran & Koch's argument is itself based on a high-Re picture that, as we have shown, can be misleading. In addition, our results do remind us that Moore's (1963) correction (4.1) to the Levich force (1.3) is relatively large even at $Re = 200$, so that the use of (1.3) or (1.1) even when there is no wake interaction may be inaccurate. While this fact would not presumably affect the qualitative results of the bubbly liquid simulations mentioned before, it might nevertheless have an impact, for example, on the speed of kinematic waves.

In agreement with Harper (1970), our calculations show that two bubbles rising in line under buoyancy will reach an equilibrium distance at which the wake effect and the

inertial repulsion balance. This fact is in marked contrast to recent experiments (Katz & Meneveau 1993), in which the bubbles have invariably been found to catch up with each other and collide. We believe that the most likely explanation of this discrepancy is to be found in the shape deformations induced by the flow which are different for the two bubbles. A numerical study of this effect along the lines of Ryskin & Leal (1984 *a*, *b*) is currently under way.

Appendix

We provide here explicit expressions for the operators introduced in §2 and their discretizations used in §3.

After expressing the differential equation for the vector potential (2.11) in bispherical coordinates and multiplying by $c^2 \sin^2 \eta$ we find the form (2.14) with

$$
\mathcal{L}_1 \psi \equiv [2 \cosh(2\mu_0 \mu)(\cos 2\eta - 1) + 4 \cosh(\mu_0 \mu)(\cos \eta - \cos 3\eta)
$$

$$
+ \cos 4\eta + 2 \cos 2\eta - 3] \left(\frac{1}{\mu_0^2} \frac{\partial^2 \psi}{\partial \mu^2} + \frac{\partial^2 \psi}{\partial \eta^2} \right)
$$

$$
+ 2[\sinh(2\mu_0 \mu)(1 - \cos 2\eta) + \sinh(\mu_0 \mu)(\cos 3\eta - \cos \eta)] \frac{1}{\mu_0} \frac{\partial \psi}{\partial \mu}
$$

$$
+ 2[-\cosh 2(\mu_0 \mu) \sin 2\eta + \cosh(\mu_0 \mu) \sin 3\eta + 5 \cosh(\mu_0 \mu) \sin \eta - 3 \sin 2\eta] \frac{\partial \psi}{\partial \eta}
$$

$$
+ 4[\cosh(2\mu_0 \mu) - 4 \cosh(\mu_0 \mu) \cos \eta + \cos 2\eta + 2] \psi. \tag{A 1}
$$

In a similar way, starting from the vorticity equation (2.12), multiplying it by $\frac{1}{2} Re \, c^2 \sin^2 \eta$, we find the form (2.15) with

$$
\mathcal{L}_2 \omega \equiv \frac{c}{\mu_0} \left\{ [\dot{c} \sinh(\mu_0 \mu) - \dot{X} \cosh(\mu_0 \mu)](\cos \eta - \cos 3\eta) + 2[-X + \mu \dot{d}](\cos 2\eta - 1) \right\} \frac{\partial \omega}{\partial \mu}
$$

$$
+ c[\dot{c} \cosh(\mu_0 \mu) - \dot{X} \sinh(\mu_0 \mu)](3 \sin \eta - \sin 3\eta) \bigg\} \frac{\partial \omega}{\partial \eta}, \tag{A 2}
$$

$$
\mathcal{N}(\omega, \psi) \equiv \frac{1}{\mu_0} [\cosh(2\mu_0 \mu)(1 - \cos 2\eta) + 2 \cosh(\mu_0 \mu)(\cos 3\eta - \cos \eta)
$$

$$
- \frac{1}{2} \cos 4\eta - \cos 2\eta + \frac{3}{2}] \left(\frac{\partial \psi}{\partial \eta} \frac{\partial \omega}{\partial \mu} - \frac{\partial \psi}{\partial \mu} \frac{\partial \omega}{\partial \eta} \right)
$$

$$
+ \frac{1}{\mu_0} [\cosh(2\mu_0 \mu) \sin 2\eta - \cosh(\mu_0 \mu) \sin 3\eta - 5 \cosh(\mu_0 \mu) \sin \eta + 3 \sin 2\eta]
$$

$$
\times \left(\psi \frac{\partial \omega}{\partial \mu} + \omega \frac{\partial \psi}{\partial \mu} \right) + [\sinh(2\mu_0 \mu)(1 - \cos 2\eta) + \sinh(\mu_0 \mu)(\cos 3\eta - \cos \eta)]
$$

$$
\times \left(\psi \frac{\partial \omega}{\partial \eta} + \omega \frac{\partial \psi}{\partial \eta} \right). \tag{A 3}
$$

We now give explicitly the discretized form of the operators introduced in §3. We use the notation

$$\mathscr{I}_{nkl} = \int_0^\pi \cos nx \sin kx \sin lx \, dx$$

$$= \tfrac{1}{4}\pi(\delta_{n-k+l,0} - \delta_{n+k-l,0} + \delta_{n-k-l,0} - \delta_{n+k+l,0}). \tag{A 4}$$

The matrix A_{kl} is given by

$$A_{kl} = 2c^2(\mathscr{I}_{0kl} - \mathscr{I}_{2kl}). \tag{A 5}$$

The operator L^1_{kl} has the expression

$$\mathrm{L}^1_{kl}\hat{\psi}_l = [2\cosh(2\mu_0\mu)(\mathscr{I}_{2kl} - \mathscr{I}_{0kl}) + 4\cosh(\mu_0\mu)(\mathscr{I}_{1kl} - \mathscr{I}_{3kl}) + \mathscr{I}_{4kl} + 2\mathscr{I}_{2kl} - 3\mathscr{I}_{0kl}]$$

$$\times \frac{1}{\mu_0^2}\frac{\partial^2 \hat{\psi}_l}{\partial\mu^2} + [2\sinh(2\mu_0\mu)(\mathscr{I}_{0kl} - \mathscr{I}_{2kl}) + 2\sinh(\mu_0\mu)(\mathscr{I}_{3kl} - \mathscr{I}_{1kl})]\frac{1}{\mu_0}\frac{\partial\hat{\psi}_l}{\partial\mu}$$

$$- l^2[2\cosh(2\mu_0\mu)(\mathscr{I}_{2kl} - \mathscr{I}_{0kl}) + 4\cosh(\mu_0\mu)(\mathscr{I}_{1kl} - \mathscr{I}_{3kl})$$

$$+ \mathscr{I}_{4kl} + 2\mathscr{I}_{2kl} - 3\mathscr{I}_{0kl}]\hat{\psi}_l + l[-2\cosh 2(\mu_0\mu)\mathscr{I}_{lk2} + 2\cosh(\mu_0\mu)\mathscr{I}_{lk3}$$

$$+ 10\cosh(\mu_0\mu)\mathscr{I}_{lk1} - 6\mathscr{I}_{lk2}]\hat{\psi}_l + 4[\cosh(2\mu_0\mu)\mathscr{I}_{0kl}$$

$$- 4\cosh(\mu_0\mu)\mathscr{I}_{1kl} + \mathscr{I}_{kl2} + 2\mathscr{I}_{0kl}]\hat{\psi}_l. \tag{A 6}$$

For the operator L^2_{kl} acting on $\hat{\omega}$ we have

$$\mathrm{L}^2_{kl}\hat{\omega}_l = \frac{c}{\mu_0}\{\dot{c}\sinh(\mu_0\mu) - \dot{X}\cosh(\mu_0\mu)](\mathscr{I}_{1kl} - \mathscr{I}_{3kl}) + 2[-\dot{X} + \mu\dot{d}](\mathscr{I}_{2kl} - \mathscr{I}_{0kl})\}\frac{\partial\hat{\omega}_l}{\partial\mu}$$

$$+ cl[\dot{c}\cosh(\mu_0\mu) - \dot{X}\sinh(\mu_0\mu)](3\mathscr{I}_{lk1} - \mathscr{I}_{lk3})\hat{\omega}_l. \tag{A 7}$$

The convolution N_k is defined by

$$N_k(\mu) = \mathscr{F}_s(k)\{\mathscr{N}(\psi, \omega)\}, \tag{A 8}$$

where $\mathscr{F}_s(k)\{\phi(\eta)\}$ extracts the kth term of the Fourier sine series for the function ϕ,

$$\mathscr{F}_s(k)\{\phi(\eta)\} = \int_0^\pi \phi(\eta)\sin k\eta \, d\eta. \tag{A 9}$$

After applying centred differences in μ, the matrices appearing in (3.4), (3.5) are readily obtained in the form

$$L^1_{ik,jl} = [2\cosh(2\mu_0\mu)(\mathscr{I}_{2kl} - \mathscr{I}_{0kl}) + 4\cosh(\mu_0\mu)(\mathscr{I}_{1kl} - \mathscr{I}_{3kl}) + \mathscr{I}_{4kl} + 2\mathscr{I}_{2kl} - 3\mathscr{I}_{0kl}]$$

$$\times \frac{\delta_{i,j-1} - 2\delta_{i,j} + \delta_{i,j+1}}{\mu_0^2\Delta\mu^2} + [2\sinh(2\mu_0\mu)(\mathscr{I}_{0kl} - \mathscr{I}_{2kl})$$

$$+ 2\sinh(\mu_0\mu)(\mathscr{I}_{3kl} - \mathscr{I}_{1kl})]\frac{\delta_{i,j+1} - \delta_{i,j-1}}{2\mu_0\Delta\mu}$$

$$- l^2[2\cosh(2\mu_0\mu)(\mathscr{I}_{2kl} - \mathscr{I}_{0kl}) + 4\cosh(\mu_0\mu)$$

$$\times (\mathscr{I}_{1kl} - \mathscr{I}_{3kl}) + \mathscr{I}_{4kl} + 2\mathscr{I}_{2kl} - 3\mathscr{I}_{0kl}]\delta_{i,j}$$

$$+ l[-2\cosh 2(\mu_0\mu)\mathscr{I}_{lk2} + 2\cosh(\mu_0\mu)\mathscr{I}_{lk3} + 10\cosh(\mu_0\mu)\mathscr{I}_{lk1} - 6\mathscr{I}_{lk2}]\delta_{i,j}$$

$$+ 4[\cosh(2\mu_0\mu)\mathscr{I}_{0kl} - 4\cosh(\mu_0\mu)\mathscr{I}_{1kl} + \mathscr{I}_{kl2} + 2\mathscr{I}_{0kl}]\delta_{i,j}, \tag{A 10}$$

$$L^2_{ik,jl} = \frac{c}{\mu_0}\{\dot{c}\sinh(\mu_0\mu) - \dot{X}\cosh(\mu_0\mu)](\mathscr{I}_{1kl} - \mathscr{I}_{3kl}) + 2[-\dot{X} + \mu\dot{d}](\mathscr{I}_{2kl} - \mathscr{I}_{0kl})\}$$

$$\times \frac{\delta_{i,j+1} - \delta_{i,j-1}}{2\Delta\mu} + cl[\dot{c}\cosh(\mu_0\mu) - \dot{X}\sinh(\mu_0\mu)](3\mathscr{I}_{lk1} - \mathscr{I}_{lk3})\delta_{i,j}, \tag{A 11}$$

where all the μ-dependent terms are evaluated at the ith node, and the convolution term N_{ik}^{n+1} in (3.5) is equation (A 8) evaluated at the same node. The δ in these equations are the Kronecker symbols.

In calculating the pressure using (2.21), the following relations are useful to find u_θ and $\partial\omega/\partial\varpi$:

$$\eta|_{\mu=-1,1} = \arctan\frac{2ca\sin\theta}{(a\cos\theta \mp \frac{1}{2}d)^2 + a^2\sin^2\theta - c^2}, \tag{A 12}$$

$$u_\theta|_{\mu=-1,1} = \frac{u_\eta(\frac{1}{2}d\cos\eta-1)\pm u_\mu c\sin\eta}{\frac{1}{2}d-\cos\eta}\cos\theta - \frac{u_\mu(1-\frac{1}{2}d\cos\eta)\pm u_\eta c\sin\eta}{\frac{1}{2}d-\cos\eta}\sin\theta, \tag{A 13}$$

$$\frac{\partial\omega}{\partial\varpi}\Big|_{\mu=-1,1} = \frac{c/a}{a\cos\eta \mp \frac{1}{2}d}\frac{1}{\mu_0}\frac{\partial\omega}{\partial\mu}\Big|_{\mu=-1,1}. \tag{A 14}$$

The explicit expression for the tangential stress boundary condition (2.17) is given by

$$2c^2(\cosh\mu_0 - \cos\eta)\,\omega|_{\mu=-1,1} = \pm(2\sinh\mu_0\cos 2\eta$$
$$- 4\sinh 2\mu_0\cos\eta + \sinh 3\mu_0 + 3\sinh\mu_0)\frac{\partial\psi}{\partial\mu} - cV^{2,1}(\cosh 2\mu_0 - 1)\sin\eta. \tag{A 15}$$

Upon taking scalar products with the set of sine functions one finds the following algebraic system:

$$2c^2\sum_{k=1}^{N}(\cosh\mu_0\mathscr{I}_{0kl} - \mathscr{I}_{1kl})\hat{\omega}_k|_{\mu=-1,1}$$
$$= \pm\sum_{k=1}^{N}[2\sinh\mu_0\mathscr{I}_{2kl} - 4\sinh 2\mu_0\mathscr{I}_{1kl} + (\sinh 3\mu_0 + 3\sinh\mu_0)\mathscr{I}_{0kl}]\frac{\partial\hat{\psi}_k}{\partial\mu}\Big|_{\mu=-1,1}$$
$$- \frac{1}{2}\pi cV^{2,1}(\cosh 2\mu_0 - 1)\delta_{1,l}. \tag{A 16}$$

REFERENCES

BATCHELOR, G. K. 1972 Sedimentation in a dilute dispersion of spheres. *J. Fluid Mech.* **52**, 245–268.

BATCHELOR, G. K. & GREEN, J. T. 1972 The determination of the bulk stress in a suspension of spherical particles to order c^2. *J. Fluid Mech.* **56**, 401–427.

BRABSTON, D. C. & KELLER, H. B. 1975 Viscous flows past spherical gas bubbles. *J. Fluid Mech.* **69**, 179–189.

CANUTO, C., HUSSAINI, M. Y., QUARTERONI, A. & ZANG, T. A. 1988 *Spectral Methods in Fluid Dynamics.* Springer.

CHEN, J. L. S. 1974 Growth of the boundary layer on a spherical gas bubble. *Trans. ASME* E: *J. Appl. Mech.* **41**, 873–878.

GRESHO, P. M. 1991 Incompressible fluid dynamics: Some fundamental formulation issues. *Ann. Rev. Fluid Mech.* **23**, 413–453.

HARPER, J. F. 1970 On bubbles rising in line at large Reynolds numbers. *J. Fluid Mech.* **41**, 751–758.

KANG, I. S. & LEAL, L. G. 1988 The drag coefficient for a spherical bubble in a uniform streaming flow. *Phys. Fluids* **31**, 233–237.

KATZ, J. & MENEVEAU, C. 1994 Wake-induced coalescence of bubbles rising in a stagnant liquid. *J. Fluid Mech.* (submitted).

KOK, J. B. W. 1989 Dynamics of gas bubbles moving through liquid. Doctoral dissertation, University of Twente, Enschede, The Netherlands.

KUMARAN, V. & KOCH, D. L. 1993a The effect of hydrodynamic interactions on the average properties of a bidispere suspension of high Reynolds number, low Weber number bubbles. *Phys. Fluids* A **5**, 1123–1134.

KUMARAN, V. & KOCH, D. L. 1993b The rate of coalescence in a suspension of high Reynolds number, low Weber number bubbles. *Phys. Fluids* A **5**, 1135–1140.

LAMB, H. 1932 *Hydrodynamics.* Cambridge University Press (reprinted by Dover).

LEVICH, V. G. 1962 *Physicochemical Hydrodynamics.* Prentice Hall.

MEI, R. & KLAUSNER, J. F. 1992 Unsteady force on a spherical bubble at finite Reynolds number with small fluctuation in the free stream velocity. *Phys. Fluids* A **4**, 233–237.

MOORE, D. W. 1963 The boundary layer on a spherical gas bubble. *J. Fluid Mech.* **16**, 161–176.

PROSPERETTI, A. 1977 On the stability of spherically symmetric flows. *Atti della Accademia Nazionale dei Lincei, Rendiconti della Classe di Scienze Fisiche, Matematiche e Naturali* **62**, 196–203.

RAMACHANDRAN, R. S., WANG, T. Y., KLEINSTREUER, C. & CHANG, H. 1991 Laminar flow past three closely spaced monodisperse spheres or nonevaporating drops. *AIAA J.* **29**, 43–51.

RYSKIN, G. & LEAL, L. G. 1984a Numerical solution of free-boundary problems in fluid mechanics. Part 1. The finite-difference technique. *J. Fluid Mech.* **148**, 1–17.

RYSKIN, G. & LEAL, L. G. 1984b Numerical solution of free-boundary problems in fluid mechanics. Part 2. Buoyancy-driven motion of a gas bubble through a quiescent liquid. *J. Fluid Mech.* **148**, 19–35.

SANGANI, A. S. & DIDWANIA, A. K. 1993a Dispersed-phase stress tensor in flows of bubbly liquids at large Reynolds numbers. *J. Fluid Mech.* **248**, 27–54.

SANGANI, A. S. & DIDWANIA, A. K. 1993b Dynamic simulations of flows of bubbly liquids at large Reynolds numbers. *J. Fluid Mech.* **250**, 307–337.

TAL, R., LEE, D. N. & SIRIGNANO, W. A. 1984 Heat and momentum transfer around a pair of spheres in viscous flow. *Intl J. Heat Mass Transfer* **27**, 1953–1962.

WIJNGARDEN, L. VAN 1993 The mean rise velocity of pairwise-interacting bubbles in liquid. *J. Fluid Mech.* **251**, 55–78.